Available online at www.sciencedirect.com

SciVerse ScienceDirect

journal homepage: www.elsevier.com/locate/jmbbm

Research paper

Effect of vacuum-treatment on deformation properties of PMMA bone cement

Fatima Zivic[a,*], *Miroslav Babic*[a], *Nenad Grujovic*[a], *Slobodan Mitrovic*[a], *Gregory Favaro*[b], *Mihaela Caunii*[b]

[a] *Faculty of Mechanical Engineering, Kragujevac, Serbia*
[b] *CSM Instruments, Switzerland*

ARTICLE INFO

Article history:
Received 16 June 2011
Received in revised form
26 July 2011
Accepted 2 August 2011
Published online 2 September 2011

Keywords:
Biomaterials
Polymethyl methacrylate (PMMA)
Bone cement
Microindentation
Deformation behavior

ABSTRACT

Deformation behavior of polymethyl methacrylate (PMMA) bone cement is explored using microindentation. Two types of PMMA bone cement were prepared. Vacuum treated samples were subjected to the degassing of the material under vacuum of 270 mbar for 35 s, followed by the second degassing under vacuum of 255 mbar for 35 s. Air-cured samples were left in ambient air to cool down and harden. All samples were left to age for 6 months before the test. The samples were then subjected to the indentation fatigue test mode, using sharp Vickers indenter. First, loading segment rise time was varied in order to establish time-dependent behavior of the samples. Experimental data showed that viscous part of the deformation can be neglected under the observed test conditions. The second series of microindentation tests were realized with variation of number of cycles and indentation hardness and modulus were obtained. Approximate hardness was also calculated using analysis of residual impression area. Porosity characteristics were analyzed using CellC software.

Scanning electron microscopy (SEM) analysis showed that air-cured bone cement exhibited significant number of large voids made of aggregated PMMA beads accompanied by particles of the radiopaque agent, while vacuum treated samples had homogeneous structure. Air-cured samples exhibited variable hardness and elasticity modulus throughout the material. They also had lower hardness values (approximately 65–100 MPa) than the vacuum treated cement (approximately 170 MPa). Porosity of 5.1% was obtained for vacuum treated cement and 16.8% for air-cured cement. Extensive plastic deformation, microcracks and craze whitening were produced during indentation of air-cured bone cement, whereas vacuum treated cement exhibited no cracks and no plastic deformation.

* *Corresponding author.*
E-mail addresses: zivic@kg.ac.rs (F. Zivic), babic@kg.ac.rs (M. Babic), gruja@kg.ac.rs (N. Grujovic), boban@kg.ac.rs (S. Mitrovic), Gregory.FAVARO@csm-instruments.com (G. Favaro), Mihaela.CAUNII@csm-instruments.com (M. Caunii).

1751-6161/$ - see front matter © 2011 Elsevier Ltd. All rights reserved.
doi:10.1016/j.jmbbm.2011.08.015

1. Introduction

Polymethyl methacrylate (PMMA) bone cement was largely used in orthopedics to anchor artificial joints. Approximately 50% of all orthopedic implants utilize bone cement to achieve implant fixation (Katti et al., 2008). Bone cement does not act as an adhesive, but rather as space filler (Reddy, 2009; Zandparsa, 2009). PMMA based materials are used for bone implants (Stojkovic et al., 2010), intraocular lenses (Kuhn, 2005), to augment the vertebral body in vertebroplasty procedure (Provenzano et al., 2004), for membranes for dialysis and complete and partial dentures (Reddy, 2009; Zandparsa, 2009). However, local tissue damage due to chemical reactions during polymerization, the high shrinkage of the cement after polymerization, the stiffness mismatch between the bone and the cement are some drawbacks associated with PMMA-based bone cements (Katti et al., 2008). Loose cement particles also mediate osteolysis of the bone. Loosening is recognized as one of the primary sources of total hip replacement failure. The fatigue failure of the implant–bone cement and bone cement–bone interface is considered to be one of the main reasons. Clinical failure of the cement occurs over long periods of time (ten years or more), and this implies that the crack growth rate is very low, perhaps as low as 10^{-12} m/cycle (Evans, 2006; Müller et al., 1997; Mohler et al., 1995; Nguyen et al., 1997; Ries et al., 2006).

Characterization of the bone cement to cyclic loading is extremely significant and is a subject of many ongoing studies (Arola et al., 2005; Briscoe et al., 2000; Evans, 2006; Gorham et al., 2003; Lewis, 2003; Stolarski and Williams, 1996). For instance, if total hip replacement is considered, daily activities involve many cycles of different alternating loading patterns (e.g. walking). Studies have shown that one of the main reasons of cement failure mechanism is related to fatigue failure and fatigue crack propagation due to cyclic stresses that can cause fatigue crack initiation and growth, further leading to the loss of structural integrity (Buckley et al., 2003; Evans, 2006; Hoey and Taylor, 2008; Lewis, 2003; Nguyen et al., 1997). However, crack propagation has not been widely studied (Buckley et al., 2003; Evans, 2006; Nguyen et al., 1997; Sinnett-Jones et al., 2005, 2008). Fatigue occurs when a material is subjected to a repeated loading and unloading. If the loads are above a certain threshold, microscopic cracks will begin to form at the surface. Eventually the crack will reach critical size, and the structure will suddenly fracture. The shape of the structure will significantly affect the fatigue life. In smooth samples, cracks initiate from pores, at the stress concentrations formed between previously polymerized PMMA beads, and there is a correlation between porosity and fatigue life (Evans, 2006; Ries et al., 2006). Fracture surfaces are formed as a consequence of the crazing process ahead of the crack tip and micromechanisms of fracture in PMMA are related to an energy dissipation zone surrounding the crack (Buckley et al., 2003; Nguyen et al., 1997). Cracks typically propagate through the PMMA beads, but in some cases it is found that the beads pull out of the matrix. It is not clear why this occurs (Evans, 2006). Despite extensive research the fatigue behavior of bone cements is not well understood.

The role of the cement is directly related to the mechanical properties of the cement, especially the resistance to fracture of the cement in the mantle at the cement–prosthesis interface or the cement–bone interface. The method of cement mixing is very important since porosity is one of the crucial characteristics that determine its resistance to fracture (Lewis, 2003; Ries et al., 2006; Sinnett-Jones et al., 2005). Inadequately mixed cement exhibits a high degree of porosity. High porosity means that a number of pores are present acting as stress raisers and initiating sites for cracks, further promoting early fatigue failure.

Vacuum mixing of the PMMA bone cement is one of the means to effectively reduce cement porosity. A number of studies have shown the benefits of this procedure over hand-mixing technique and investigated different parameters affected by the application of vacuum mixing (Hoey and Taylor, 2008; Lelovics and Liptakova, 2010; Lewis, 2011). However, the optimum level of vacuum and the optimum porosity in the cement are still under debate. For instance, Hoey and Taylor (2008) reported that vacuum mixing technique, even though it reduced porosity, resulted in no significant improvement of fatigue strength. Sinnett-Jones et al. (2008) showed that large agglomerations of additional constituents in bone cement (such as particle size additives) are subject to microcracking during fatigue, although in the majority of cases, these are not the primary cause of failure. They concluded that even though pores acted as stress raisers and initiating sites for cracks, porosity and local additives distribution acted together in crack formation.

Depth-sensing indentation techniques are used routinely to measure mechanical properties. They offer experimental control allowing investigation of a variety of different deformation modes by changing experimental time scale, indenter tip geometry, and loading conditions (Bhuhsan and Li, 2003; Gouldstone et al., 2007; Myshkin, 2004; Oyen, 2006; Oyen and Cook, 2009). Microindentation technique is an already established method, in which the load, F, and displacement, h, are monitored during the contact of an indenter tip with a known geometry and a material surface. When reaching a pre-set maximum value, the normal load is reduced until partial or complete relaxation occurs. Indentation with the constant multicycle mode represents the fatigue mode of testing. However, it is very important to determine the appropriate analysis of indentation data according to the material deformation modes which occur during indentation (Bhuhsan and Li, 2003; Oyen, 2006; Oyen and Cook, 2009).

We report some experimental work regarding the preparation procedure of PMMA bone cement and investigate the influence of the vacuum treatment of hand-mixed PMMA bone cement on its deformation behavior during microindentation. We analyzed deformation modes of PMMA bone cement prepared in two different ways: vacuum treated and air-cured samples.

2. Material and methods

2.1. Materials

Commercially available PMMA bone cement for orthopedic surgery (Palacos R, Schering Corporation, Kenilworth, New

Table 1 – Composition of PMMA bone cement.

Polymer powder components		Liquid components (monomer)	
Constituent	Mass (g)	Constituent	Mass (g)
Methylacrylate—Copolymer	33.80	MMA (Methylmethacrylate), stabilized with Hydroquinone	18.4
Benzylperoxide	0.20	N, N-Dimethyl-p-toluidine	0.4
Zirconiumdioxide	6.00	Chlorophyll	0.005
Chlorophyll	0.008		

Table 2 – The phases of the preparation procedure of the vacuum treated and the air-cured bone cement.

Phase	Preparation procedure	Time
1.	Hand mixing by using spatula	1 min 35 s
2.	Mixing by using hand mixer	2 min 45 s
3.	Degassing of the material in a vacuum chamber (450 mbar)	35 s
	Vacuum treated bone cement	Air-cured bone cement
4.	Degassing of the material in a vacuum chamber (270 mbar) for 35 s	Curing of the cement (ambient air, temperature of 25 °C and relative humidity of 40%)
5.	Degassing of the material in a vacuum chamber (255 mbar) for 35 s	
6.	Curing of the cement (ambient air, temperature of 25 °C and relative humidity of 40%)	

Jersey, USA) was used as a test material. PMMA is an isotropic, showing no crystallinity, elasto-viscoplastic solid and an amorphous polymer. Composition of used PMMA bone cement is given in Table 1.

Bone cement was mixed according to the manufacturer's instructions. Polymer powder was poured into a stainless steel container and liquid monomer was added after that. Powder component stayed in open air for 2 min before being mixed with the liquid component. At the beginning, mixing of the two components was done using a spatula (1 min 35 s duration) and then by using a small hand mixer in ambient air (2 min 45 s total mixing time). After that, the material was of light dough consistency. Then, stainless steel container with the material was held in a vacuum chamber for 35 s (under vacuum of 450 mbar). Extensive light gray smoke coming out of the container indicated degassing of the material. The vacuum chamber of Vacuum casting system MCP 5.01 (MTT Technologies GmbH, Lübeck, Germany) was used to degas prepared material.

Plastic molds (according to ASTM F451-99 "Standard Specifications for Acrylic Bone Cements") were filled with the material to form samples. One set of plastic molds containing the material was then returned into the vacuum chamber: (1) under vacuum of 270 mbar for 35 s and (2) under vacuum of 255 mbar for 35 s. After that, molds with the material were left in ambient air (temperature of 25 °C and relative humidity of 40%) to cool and harden. Further in the text, this group of samples is referred to as vacuum treated bone cement, VT. The second group of molds was just left in ambient air to cool and harden. Further in the text, this group of samples is referred to as air-cured bone cement, AC. Total time of preparation after opening the powder and liquid components was 10 min 9 s. Table 2 shows phases of the preparation procedure of two groups of bone cements.

All samples were left to age for 6 months before the test. The properties of PMMA bone cements as a function of aging time are important (Lewis et al., 2007; Provenzano et al., 2004). Passage of time reduces creep rate (Lee et al., 2002; Lewis, 2011). In the case of some laboratory-prepared bone cements, the aging time of one month produced steady state values of elasticity modulus and hardness (Lewis et al., 2007; Nottrott et al., 2007). However, there is a lack of consensus on the influence of either real-time *in vitro* or *in vivo* aging on the properties of PMMA bone cement (Lewis et al., 2007; Lewis, 2011).

Samples were stored in a closed desiccator, at approximate 22 °C. Prior to the tests, all samples were polished to the roughness of $Ra = 10.5$ μm. The morphological study of the control samples was carried out by using a low vacuum Jeol JSM-6610LV scanning electron microscope equipped with Everhart–Thornley detector for Secondary Electron (SE) imaging, Backscatter electron (BSE) detector, and Energy Dispersive (EDS) detector (X-Max Large Area Analytical Silicon Drift connected with INCAEnergy 350 Microanalysis System). Resulting SEM images were digitally processed (with freeware CellC software for spot analysis) to determine the average size, number and density of voids. Density of voids (number/μm^2) was determined for three control surfaces and averaged, for each sample. Porosity was calculated for both types of samples according to the data obtained from CellC software analysis.

2.2. *Instrumented indentation testing*

Indentations were performed on each sample using the Micro Indentation Tester (CSM Instruments SA, Peseux, Switzerland). The tests were performed with a maximum normal load of 15 N and a minimum load of 5 N, using sharp indentation (Vickers indenter). Large (deep) indentations were analyzed, avoiding effects due to the tip shape uncertainty. There was no pause at maximum load before unloading (fatigue mode of testing). Two series of tests were realized. First, the time to maximum load was changed (loading segment rise time) under the same number of cycles (100 cycles) to determine time dependent properties of prepared bone cement

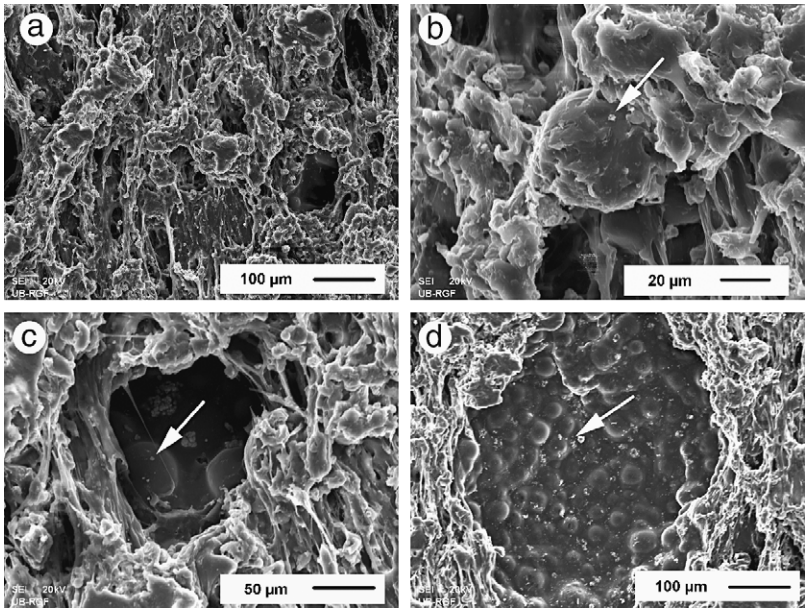

Fig. 1 – SEM photographs. (a) Sample surface of the vacuum treated bone cement. (b) Partially dissolved surface of spherical pre-polymerized PMMA beads. (c) One of the largest voids on the surface of the vacuum-treated cement. (d) Large void on the surface of the air-cured cement.

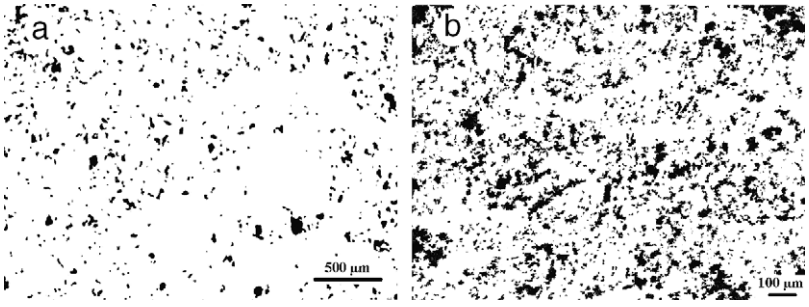

Fig. 2 – Void density (as obtained from CellC software after SEM images processing): (a) vacuum treated bone cement; (b) air-cured bone cement.

at these test conditions. Then, the number of indentation cycles was varied at time to a maximum load of 30 s.

During indentation test, the depth, h, to which the indenter penetrated the surface (equal to the displacement of the indenter), was recorded as a function of the indenter load, F. The values of the indentation testing hardness, H_{IT} and indentation modulus, E_{IT} were automatically calculated and recorded by the device using the Oliver and Pharr method. It is the most common approach to determine hardness and modulus by interpretation of load–penetration depth (F–h) behavior during indentation (Oliver and Pharr, 1992).

The indentation testing hardness, H_{IT} is determined from the maximum load, F_{max} divided by the projected contact area, A_p at the contact depth, h_c:

$$H_{IT} = F_{max}/A_p(h_c) \quad (1)$$

where h_c is the depth of the contact of the indenter with the sample at F_{max}. A_p is a function of the contact depth h_c. The Vickers hardness HV, for Vickers indenter is defined by: HV = $0.0945H_{IT}$. Young's modulus of the sample, i.e. indentation modulus E_{IT}, is obtained from:

$$1/E_r = (1-\nu_s^2)/E_{IT} + (1-\nu_i^2)/E_i \quad (2)$$

where:

ν_s is the Poisson ratio of the sample,
ν_i is the Poisson ratio of the indenter,
E_r is the reduced modulus of the indentation contact, which depends on the projected contact area A_p, the contact stiffness and the indenter geometry
E_i is the modulus of the indenter.

3. Results

Fig. 1 shows details of the sample surfaces prior to the tests. Fig. 2 is obtained by using CellC software and indicates void density and distribution of void size on VT and

Table 3 – Average size, number and density of voids.

Size of the voids (μm)	Vacuum-treated bone cement Porosity: 5.1% (in average, 114 voids/mm^2)		Air-cured bone cement Porosity: 16.8% (in average, 1414 voids/mm^2)	
	Distribution of voids: 674 voids per 5.9 mm^2 (control surface)		Distribution of voids: 1980 voids per 1.4 mm^2 (control surface)	
	Number of voids	Average void size (μm)	Number of voids	Average void size (μm)
<10	222	6	1422	5
>10 and <50	415	21	465	21
>50 and <100	28	66	66	71
>100	9	124	27	140

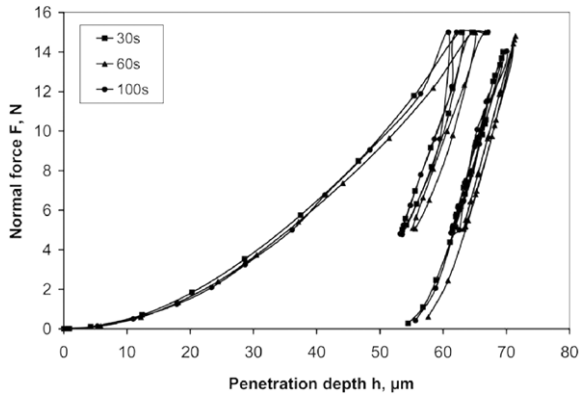

Fig. 3 – Indentation curves (the beginning and ending part) of the vacuum treated bone cement for three different times to maximum load: 30, 60, 100 s.

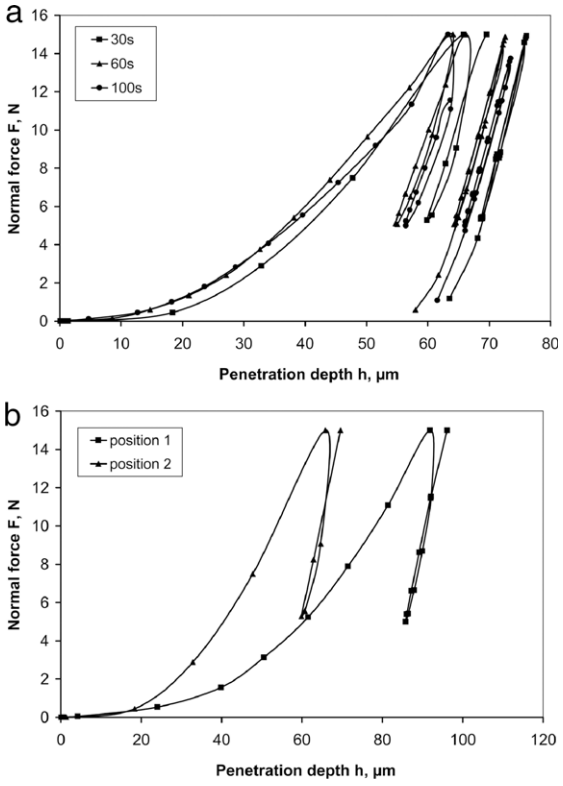

Fig. 4 – Indentation curves (the beginning and ending part) of the air-cured bone cement for: (a) three different times to maximum load (30, 60, 100 s); (b) two different indentation positions at time to maximum load of 30 s.

AC samples. Vacuum treated samples exhibited uniform structure (Fig. 1(a)) with significantly smaller number of voids than samples that were only air-cured (Fig. 1(d)). The voids observed on VT sample were of much smaller dimensions (Fig. 1(c)) if compared to the voids on AC sample (Fig. 1(d)). The surface of the VT sample mainly exhibited the structure as shown in Fig. 1(a). Different inhomogeneities were observed on the surface of the AC sample, even after the polishing: (1) large voids occupying a significant fraction of area; (2) number of small voids; (3) shallow cavities consisting of small-sized voids and partially dissolved pre-polymerized PMMA bead, and (4) aggregated undissolved PMMA beads surrounded by particulate radiopaque agent (Fig. 1(b)). Partially dissolved surface of spherical pre-polymerized PMMA beads is shown in Fig. 1(b).

Table 3 presents porosity characteristics of vacuum treated and air-cured bone cement samples.

Fig. 3 shows indentation curves of the vacuum treated bone cement, that is, the diagram of the normal force applied during micro indentation as a function of the penetration depth, for different rise times. Fig. 4 shows indentation curves of the air-cured bone cement, for different rise times. It should be noted that the repeated indentation test on AC cement produced significantly higher maximum penetration depth than the first test (Fig. 4(b)). Figs. 3 and 4(a) present only the beginning and ending part of the indentation curves, for reason of better visibility. The total mechanical work induced by the indentation is consumed as plastic deformation work and elastic reverse deformation work of indentation. The ratio of the plastic deformation work to the total work was automatically calculated during the indentation (Fig. 5).

Fig. 6 shows the indentation curves of the vacuum treated bone cement at three different number of cycles. Fig. 7 shows the indentation curves of the air-cured bone cement at three different number of cycles. Nonpredictive indentation behavior of the air-cured bone cement, exhibited in Fig. 4(b), can also be noticed in Fig. 7. The lowest penetration depth was obtained in case of 200 cycles (Fig. 7).

Table 4 presents the mean values of indentation hardness, H_{IT} and elastic modulus, E_{IT} automatically obtained by the indentation tester. These values (H_{IT}, E_{IT}) are calculated according to Oliver and Pharr approach, by analyzing the unloading part of the curve (Figs. 6 and 7). Good agreement with known values of hardness and modulus as per the literature was obtained.

Table 4 – Mean values of indentation hardness, H_{IT} elastic modulus, E_{IT} and hardness, H of the bone cement samples (time to maximum load of 30 s).

Number of indentation cycles	Vacuum treated bone cement			Air-cured bone cement		
	100	200	300	100	200	300
Hardness (as obtained by the indenter), H_{IT} (MPa)	178.99	175.45	162.84	89.33	96.95	65.49
Hardness, H calculated from imprint area size (MPa)	174.4	171.5	151.2	104.4	93.75	81.7
Elastic modulus, E_{IT} (GPa)	2.90	2.91	2.74	2.10	2.96	2.08

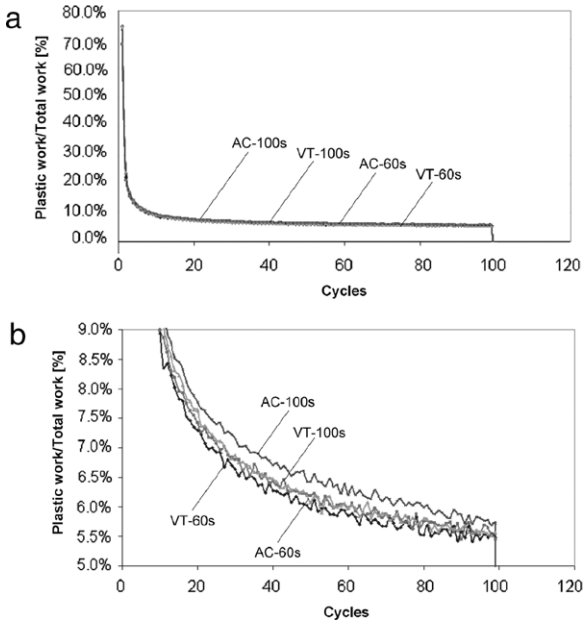

Fig. 5 – (a) Ratio of the plastic deformation work to the total work during indentation for VT and AC samples at different rise times (60, 100 s). (b) Enlarged portion of the curve.

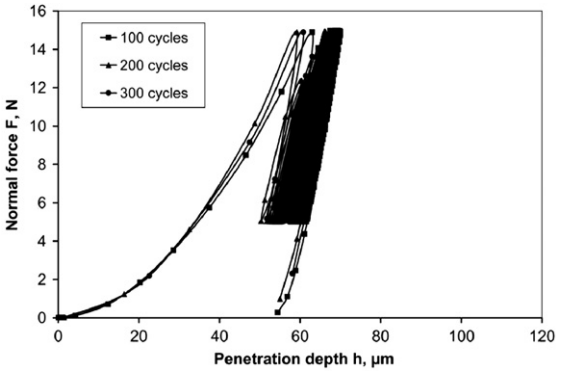

Fig. 6 – Indentation curves of the vacuum treated bone cement at time to maximum load of 30 s, for three different numbers of cycles: 100, 200, 300 cycles.

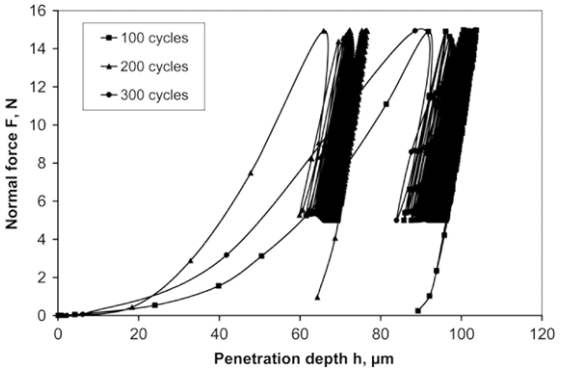

Fig. 7 – Indentation curves of the air-cured bone cement at time to maximum load of 30 s, for three different number of cycles: 100, 200, 300 cycles.

Fig. 8 shows optical micrographs of the indentation imprints on the vacuum treated bone cement, after indentation. Typical pattern produced by Vickers indentation is clearly seen. The imprints are well shaped with clearly developed edges and no microcracks along edges. Fig. 9 presents optical micrographs of the indentation imprints on the air-cured bone cement, after indentation. Indentation imprints in Figs. 8 and 9 are significantly different. Extensive plastic deformation is exhibited in Fig. 8, especially pronounced in the corner areas (denoted by the circle in Fig. 9(b)). Also, stress whitening and microcracks can be observed along the imprint edges (denoted by arrows in Fig. 9).

The length of each side of the quadratic residual impressions (Figs. 8, 9) was measured from the optical images and averaged for each imprint. An approximate area, A was calculated, assuming the quadrant area with side length equal to the average of the four measured lengths. Table 4 shows approximate hardness values, H calculated by $H = F_{max}/A$.

4. Discussion

Figs. 6 and 7 indicate that substantial energy dissipation in a single cycle was realized for both tested samples of bone cement, but it was larger for air-cured samples than for vacuum treated material. Hardness and modulus are both influenced by time-dependent effects and cannot be simply determined using standard techniques, e.g. Oliver and Pharr (Lee et al., 2002; Lewis et al., 2006; Oyen and Cook, 2002; Oyen, 2006; Oyen and Cook, 2009; Provenzano et al., 2004). However, in case of experimental conditions in our study, the unloading segments of the F–h curve for both bone cement samples did not exhibit time-dependent responses (Figs. 3 and 4), that is, a forward-displacing "nose" (Lee et al., 2002; Oyen and Cook, 2002; Oyen, 2006; Oyen and Cook, 2009). It means that in the case of our experimental conditions, hardness and modulus can be calculated according to Oliver and Pharr approach. In the case of air-cured cement, these values should probably be taken with some uncertainty due to uneven distribution within the material (Figs. 1(d) and 2(b)). Hardness values

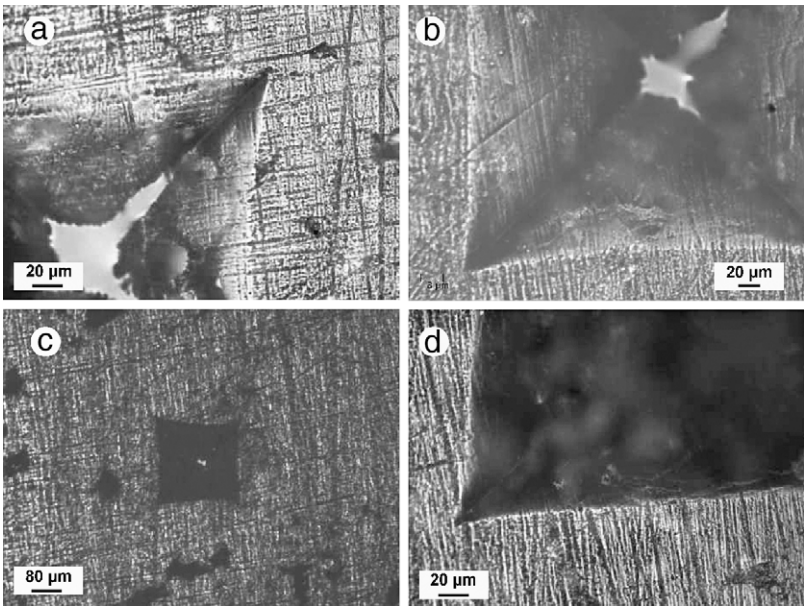

Fig. 8 – Optical micrographs of the indentation imprint on the vacuum treated bone cement after: (a) 100 cycles, (b), (c) 200 cycles and (d) 300 cycles.

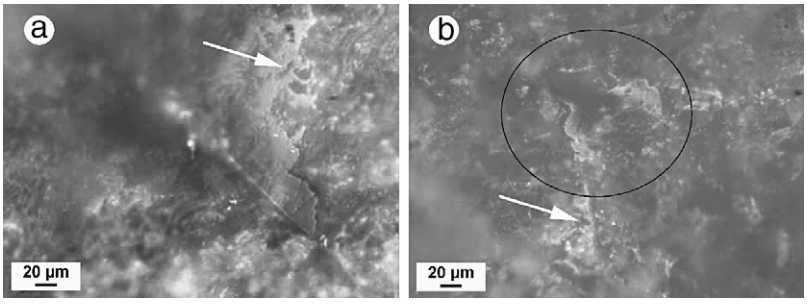

Fig. 9 – Optical micrographs of the indentation imprint on the air-cured bone cement after 100 cycles and at two different times to maximum load: (a) 30 s, (b) 60 s.

for air-cured bone cement were significantly lower than for vacuum treated material, as expected according to the SEM analysis of sample surface (Figs. 1 and 2).

Ying (2007) proved that viscosity of the PMMA material strongly responds to the applied strain rate or loading rate. Lewis (2011) investigated influences of factors, such as cement composition, loading rate and the cement mixing method on the viscosity–time profile of PMMA bone cement and reported that different factors can be used to obtain desired profile of viscosity–time of the cement mixture. Considering Figs. 3–5, it can be concluded that the influence of the viscous part of material behavior is negligible for the applied range of experimental conditions. The curves representing part of the plastic deformation work during indentation (Fig. 5) coincide to each other additionally indicating that the influence of the viscous part can be neglected in this case. Oyen (2006) showed that the degree of influence of time-dependent deformation of PMMA can be simply determined by the change of the residual imprint size in indentation tests when loading time is varied. Residual indentation areas after tests where rise time was varied (30, 60, 100 s) were approximately of the same size in our tests, also indicating that viscous deformation can be neglected for our experimental conditions. Hardness values, H that were calculated from residual impressions were congruent with the values of indentation hardness, H_{IT} obtained by the indentation tester (Table 4). However, in the case of air-cured cement, indentation behavior was influenced by the indentation position on the sample surface. Indentation curve of the test under 200 cycles, is displaced to the left as compared to the other two curves (100, 300 cycles), as shown in Fig. 7. This can be due to the influence of the increased number of voids as shown in Fig. 2, leading to rather unpredictable indentation behavior of air-cured bone cement.

The pre-polymerized PMMA beads in bone cement powder are approximately spherical (Liu et al., 2001). Monomer dissolves smaller particles of the polymer and partially dissolves the surface of the bigger particles incorporating them uniformly in the cured bone cement as shown in Fig. 1(a) and (b). However, throughout the cured bone cement certain voids can always be observed (Fig. 2). SEM analysis showed that the large voids were due to agglomeration of

undissolved big PMMA beads such as in Fig. 1(c) and (d). These types of voids were observed in both types of samples but in significantly higher extent on the surface of the air-cured bone cement. Also, voids observed on VT cement were of small dimensions (Fig. 1(c)), unlike the large voids on AC cement samples (Fig. 1(d)). The surface of the VT cement was mainly like as shown in Fig. 1(a), while the surface of the AC cement exhibited significant proportion of the large particles that remained undissolved such as in Fig. 1(d). Voids are formed by air trapped during mixing and are monomer deficient. According to many realized studies these defects reduce the mechanical strength and represent high stress concentration which lead to early cement fracture (Hoey and Taylor, 2008; Lewis et al., 2007; Liu et al., 2001). It was expected that the air-cured cement exhibit lower hardness and elastic modulus in microindentation tests.

The smallest particles (size range <1 μm) (small white particles denoted by arrow in Fig. 1(d)) represent the radiopaque agent: zirconium dioxide in Palacos R bone cement. Palacos R bone cement contains nearly 15% of the radiopaque agent (Liu et al., 2001). SEM analysis of the samples' surface showed how the small radiopaque particles adhere to and fill the spaces between the relatively large pre-polymerized PMMA beads, as presented in Fig. 1 (denoted by the arrow). Higher concentrations of radiopaque additive influence the impact strength decrease of the bone cement (Lelovics and Liptakova, 2010; Liu et al., 2001; Oyen and Cook, 2002). Agglomeration of undissolved PMMA beads accompanied by particles of radiopaque agent (Fig. 1(c) and (d)) significantly influences the mechanical properties of the bone cement, according to the results in this study (Table 4).

Indentations on vacuum treated cement produced a smooth surface (Fig. 8), unlike the rough surfaces exhibited in the case of air-cured samples (Fig. 9). Increased surface roughness influences microscopic stress concentrations that lower the fatigue strength and represent a source of fatigue cracks and failure. In the case of air-cured cement, both the increase in the number of cycles, as well as the increase in the rise time, produced the increase in the residual imprint surface roughness (Fig. 9). Visual examination of the imprint on the air-cured cement (Fig. 9) revealed stress whitening arising from the development of crazes before crack propagation, under all test conditions. The imprint surface was fragmented with microcracks (denoted by the arrow in Fig. 9). Microstructural properties of bone cement affect the fracture or failure mechanism (Hoey and Taylor, 2008; Lee et al., 2002; Liu et al., 2001). When the polymerization process of the liquid monomer is finished, matrix polymer is surrounding the PMMA beads as in Fig. 1(a) and (b). Molecular weight of interstitial matrix polymer is much higher than that of PMMA beads (Provenzano et al., 2004; Liu et al., 2001). This difference also exists between the matrix polymer and the radiopaque agent and altogether may result in the difference in elastic modulus. This, in return, may cause contact stress at the interfacial zone between the matrix and the beads, especially in parts where PMMA beads remained undissolved. It might lead to the partial debonding of the PMMA beads from the matrix and microcrack nucleation in the cement structure.

Liu et al. (2001) investigated failure modes of air-cured bone cement and proved that compressive loads produced yield and plastic deformation, leading to "yield cracks" after some critical load. Results of the indentation tests in our studies are in accordance with their findings showing evidence of yield and plastic deformation (Fig. 9), accompanied by the craze whitening which indicates further cracks. Air-cured cement undergone considerable plastic deformation without failure, even though microcracks occurred (Fig. 9). This is in consistence with findings of Baran et al. (1994), who investigated indentation cracking of polymer matrix materials. In the case of air-cured cement, large variations of hardness and elasticity modulus were obtained (Table 4). Hardness implies resistance to local deformation. Significantly lower values of hardness were obtained for AC than for VT cement (Table 4), and AC cement exhibited extensive deformation (Fig. 9). Hoey and Taylor (2008) investigated the influences of different defects and stress concentrations in bone cement on its fatigue strength. They reported that clusters of pores were seen at crack initiation sites, indicating that defects in a form of voids provoke failure. This is in accordance with our findings where voids of aggregated PMMA beads accompanied by particles of radiopaque agent, probably represented stress concentrations.

Unlike the air-cured cement, vacuum treated cement exhibited small number of large voids made by aggregated PMMA beads (Figs. 1, 2). Also, SEM analysis indicated that these voids were of much smaller dimensions in the case of VT cement than for AC cement. Consequently, VT cement exhibited better mechanical characteristics (higher hardness and modulus) due to lower number of stress initiators. VT cement did not exhibit craze whitening, indicating that it is less prone to fracture and failure. VT cement showed no cracking after indentation for all test conditions (variation of rise time and number of cycles). There were no cracks extending from the corners of the imprint and no visible plastic deformation occurred either. Petit et al. (2007) stated that in order for results of instrumented indentation to be reliable, deleterious effects of micro-cracking and occurrence of macro cracks (e.g. from corners of the imprint) should be avoided. Thus, obtained results of hardness for vacuum treated samples can be taken as reliable, whereas in the case of air-cured samples some additional methods should be engaged to obtain correct hardness values.

Fatigue behavior is influenced by many parameters such as: applied fluctuating stress, environment, presence of residual stresses, surface condition, stress concentration and imperfections in the material. In this investigation, two different preparation procedures of PMMA bone cement produced significantly different behavior. Surface damage occurring in the micro-load range greatly affects the indentation response (deformation mode) of the material and consequently the values of the material hardness and Young's modulus. Since applied loads and environment were the same for both samples, obtained difference in the deformation behavior can be attributed to the forming of voids and stress concentrations during curing, due to the aggregation of undissolved PMMA beads accompanied by radiopaque agent particles.

5. Conclusions

Vacuum treatment of hand-mixed polymethyl methacrylate (PMMA) bone cement produced excellent results in regard to the mechanical characteristics. Vacuum treated PMMA bone cement exhibited homogeneous structure. Air-cured bone cement had rather unpredictable microindentation behavior due to significant number of large voids made of aggregated PMMA beads accompanied by particles of radiopaque agent. Variable hardness and elasticity modulus were obtained over the surface of the air-cured bone cement. It had lower hardness values than vacuum treated cement, corresponding to extensive plastic deformation. Air-cured bone cement also exhibited microcracks and craze whitening. Vacuum treated bone cement showed no cracks and no plastic deformation after indentation.

Acknowledgment

The results of this paper are realized through the national project TR-35021 financially supported by the Ministry of Science of the Republic of Serbia.

REFERENCES

Arola, D., Stoffel, K.A., Yang, D.T., 2005. Fatigue of the cement/bone interface: the surface texture of bone and loosening. J. Biomed. Mater. Res. Part B 76B, 287–297.

Baran, G., Shin, W., Abbas, A., Wunder, S., 1994. Indentation cracking of composite matrix materials. J. Dent. Res. 73, 1450–1456.

Bhuhsan, B., Li, X., 2003. Nanomechanical characterisation of solid surfaces and thin films. Int. Mater. Rev. 48, 125–164.

Briscoe, B.J., Chateauminois, A., Lindley, T.C., Parsonage, D., 2000. Contact damage of poly(methylmethacrylate) during complex microdisplacements. Wear 240, 27–39.

Buckley, P.J., Orr, J.F., Revie, I.C., Breusch, S.J., Dunne, N.J., 2003. Fracture characteristics of acrylic bone cement–bone composites. Proc. Inst. Mech. Eng. Part H J. Eng. Med. 217, 419–427.

Evans, S.L., 2006. Fatigue of PMMA bone cement, fracture of nano and engineering materials and structures. In: Gdoutos, E.E. (Ed.), Fracture of Nano and Engineering Materials and Structures. In: Proceedings of the 16th European Conference of Fracture, Springer, pp. 271–272.

Gorham, D.A., Salman, A.D., Pitt, M.J., 2003. Static and dynamic failure of PMMA spheres. Powder Technol. 138, 229–238.

Gouldstone, A., Chollacoop, N., Dao, M., Li, J., Minor, A.M., Shen, Y.L., 2007. Indentation across size scales and disciplines: recent developments in experimentation and modeling. Acta Mater. 55, 4015–4039.

Hoey, D., Taylor, D., 2008. Fatigue in porous PMMA: the effect of stress concentrations. Int. J. Fatigue 30, 989–995.

Katti, K.S., Verma, D., Katti, D.R., 2008. Materials for joint replacement. In: Revell, P.A. (Ed.), Joint Replacement Technology. Woodhead Publishing Limited, p. 90. (Chapter 4).

Kuhn, L.T., 2005. Biomaterials. In: Enderle, J.D., Bronzino, J.D., Blanchard, S.M. (Eds.), Introduction to Biomedical Engineering. Elsevier Academic Press, Oxford, pp. 256–263. (Chapter 6).

Lee, A.J.C., Ling, R.S.M., Gheduzzi, S., Simon, J.P., Renfro, R.J., 2002. Factors affecting the mechanical and viscoelastic properties of acrylic bone cement. J. Mater. Sci., Mater. Med. 13, 723–733.

Lelovics, H., Liptakova, T., 2010. Time and mixing technique-dependent changes in bone cement smartset§HV. Acta Bioeng. Biomech. 12, 63–67.

Lewis, G., 2003. Fatigue testing and performance of acrylic bone–cement materials: state-of-the-art review. J. Biomed. Mater. Res. Part B 66B, 457–486.

Lewis, G., 2011. Viscoelastic properties of injectable bone cements for orthopaedic applications: state-of-the-art review. J. Biomed. Mater. Res. Part B Appl. Biomater. 98, 171–191.

Lewis, G., Xu, J., Dunne, N., Daly, C., Orr, J., 2006. Critical comparison of two methods for the determination of nanomechanical properties of a material: application to synthetic and natural biomaterials. J. Biomed. Mater. Res. Part B Appl. Biomater. 78, 312–317.

Lewis, G., Xu, J., Dunne, N., Daly, C., Orr, J., 2007. Evaluation of an accelerated ageing medium for acrylic bone cement based on analysis of nanoindentation measurements on laboratory-prepared and retrieved specimens. J. Biomed. Mater. Res. Part B 81, 544–550.

Liu, C., Green, S.M., Watkins, N.D., Gregg, P.J., McCaskie, A.W., 2001. Some failure modes of four clinical bone cements. Proc. Inst. Mech. Eng., Part H 215, 359–366.

Mohler, C.G., Callaghan, J.J., Collis, D.K., Johnston, R.C., 1995. Early loosening of the femoral component at the cement–prosthesis interface after total hip replacement. J. Bone Joint Surg. A 77, 1315–1322.

Müller, R.T., Heger, I., Oldenburg, M., 1997. The mechanism of loosening in cemented hip prostheses determined from long-term results. Arch. Orthop. Trauma Surg. 116, 41–45.

Myshkin, N.K., 2004. Devices for tribotests at micro/nano scale. Tribology in Industry 26, 15–20.

Nguyen, N.C., Maloney, W.J., Dauskardt, R.H., 1997. Reliability of PMMA bone cement fixation: fracture and fatigue crack-growth behaviour. J. Mater. Sci., Mater. Med. 8, 473–483.

Nottrott, M., Mølster, A.O., Gjerdet, N.R., 2007. Time dependent mechanical properties of bone cement. An in vitro study over one year. J. Biomed. Mater. Res. Part B Appl. Biomater. 83, 416–421.

Oliver, W.C., Pharr, G.M., 1992. An improved technique for determining hardness and elastic modulus using load and displacement sensing indentation experiments. J. Mater. Res. 7, 1564–1583.

Oyen, M.L., 2006. Analytical techniques for indentation of viscoelastic materials. Phil. Mag. 86, 5625–5641.

Oyen, M.L., Cook, R.F., 2002. Load–displacement behavior during sharp indentation of viscous-elastic-plastic materials. J. Mater. Res. 18, 139–150.

Oyen, M.L., Cook, R.F., 2009. A practical guide for analysis of nanoindentation data. J. Mech. Behav. Biomed. Mater. 2, 396–407.

Petit, F., Vandeneede, V., Cambier, F., 2007. Relevance of instrumented micro-indentation for the assessment of hardness and Young's modulus of brittle materials. Mater. Sci. Eng. A 456, 252–260.

Provenzano, M., Murphy, K.P.J., Riley III, L.H., 2004. Bone cements: review of their physiochemical and biochemical properties in percutaneous vertebroplasty. AJNR Am. J. Neuroradiol. 25, 1286–1290.

Reddy, N.R., 2009. Design of artificial kidneys. In: Kutz, M. (Ed.), Biomedical Engineering and Design Handbook, vol. 2. McGraw-Hill, New York, pp. 149–150. (Chapter 5).

Ries, M.D., Young, E., Al-Marashi, L., Goldstein, P., Hetherington, A., Petrie, T., Pruitt, L., 2006. In vivo behavior of acrylic bone cement in total hip arthroplasty. Biomaterials 27, 256–261.

Sinnett-Jones, P.E., Browne, M., Ludwig, W., Buffiére, J.-Y., Sinclair, I., 2005. Microtomography assessment of failure in acrylic bone cement. Biomaterials 26, 6460–6466.

Sinnett-Jones, P.E., Browne, M., Moffat, A.J., Jeffers, J.R.T., Saffari, N., Buffiére, J.Y., Sinclair, I., 2008. Crack initiation processes in acrylic bone cement. J. Biomed. Mater. Res. Part A 89A, 1088–1097.

Stojkovic, M., Milovanovic, J., Vitkovic, N., Trajanovic, M., Grujovic, N., Milivojevic, V., Milisavljevic, S., Mrvic, S., 2010. Reverse modeling and solid free-form fabrication of sternum implant. Australas. Phys. Eng. Sci. Med. 33, 243–250.

Stolarski, T.A., Williams, H., 1996. Mode of loading and contact configuration effects in the wear of polymers. J. Appl. Polym. Sci. 61, 1217–1222.

Ying, S., 2007. Rheologic fracture of PMMA material at different strain rates. J. Cent. South. Univ. Technol. 14, 342–345.

Zandparsa, R., 2009. Dental biomaterials. In: Kutz, M. (Ed.), Biomedical Engineering and Design Handbook, vol. 1. McGraw-Hill, New York, p. 405. (Chapter 17).